Interday Reliability of Upper-limb Geometric MyoPassivity Map for Physical Human-Robot Interaction

Xingyuan Zhou*, *Student Member, IEEE,* Peter Paik*, *Student Member, IEEE,*
Rory O'Keeffe*, *Student Member, IEEE,* S. Farokh Atashzar†, *Senior Member, IEEE*

***Abstract*—The value of intrinsic energetic behavior of human biomechanics has recently been recognized and exploited in physical human-robot interaction (pHRI). The authors have recently proposed the concept of "Biomechanical Excess of Passivity," based on nonlinear control theory, to construct a user-specific energetic map. The map would assess the behavior of the upper-limb in absorbing the kinesthetic energy when interacting with robots. Integrating such knowledge into the design of pHRI stabilizers can reduce the conservatism of the control by unleashing hidden energy reservoirs indicating a less conservative margin of stability. The outcome would enhance the system's performance, such as rendering kinesthetic transparency of (tele)haptics systems. However, current methods require an offline data-driven identification procedure prior to each operation to estimate the energetic map of human biomechanics. This can be time-consuming and challenge users susceptible to fatigue. In this study, for the first time, we investigate the interday reliability of upper-limb passivity maps in a sample of five healthy subjects. Our statistical analyses indicate that the identified passivity map is highly reliable in estimating the expected energetic behavior based on Intraclass correlation coefficient analysis (conducted on different days and with various interactions). The results illustrate that a one-shot estimate is a reliable measure to be used repeatedly in biomechanics-aware pHRI stabilization, enhancing practicality in real-life scenarios.**

***Index Terms*—Physical Human-Robot Interaction, Energetic Behavior, Passivity, Test-retest Reliability, Biomechanics.**

I. Introduction

The concept of human-robot coexistence has gained widespread attraction in the current decade, highlighting the importance of physical human-robot interaction (pHRI). Therefore, increasingly more pHRI scenarios have emerged, from robotic exoskeletons used in assistive systems to rehabilitative robotics and telerobotics-assisted surgical systems [1]–[4]. In order to provide better quality for pHRI and specifically haptics-enabled pHRI, two essential factors should be practiced: (1) maximizing safety during pHRI and (2) optimizing the fidelity of interactional information transfer between robot mechanics and human biomechanics. The safety of haptics-enabled pHRI systems is impacted by several features, including poor quality of energy transfer. Passivity theory governs energy exchange between robots and humans in a pHRI scenario [5]–[7]. Any (a) internal phenomenon, such as sensor noise and actuators' fault, or (b) external phenomenon, such as prescribed assistive haptics/force field or delays and packet losses (in a telehaptic formulation) that injects energy in the coupling, or disturbs the synchronicity and consistency of energy exchange can result in a nonpassive coupling between human and robot, which could cause undesirable oscillating behavior and possibly can even cause divergent instability in the system, challenging the safety of the pHRI [8]–[10].

As a result, a guaranteed safety layer should be embedded into the pHRI control architecture to ensure the system's stability when exposed to internal and external nonpassive safety blocks. In the literature, various stabilizers have been proposed (depending on the pHRI architecture) that impose stability. A widely-used and efficient method for handling uncertain environmental dynamics and variable delays are the Time-domain Passivity Approach (TDPA) [11]–[17]. The family of TDPA stabilizers observes the system energy by monitoring the exchange of power packets (or energy profile) between different components of the system to adaptively modulate a control parameter (e.g., a damping or scaling factor) to tune the exchanged information and dissipate the excess energy, ensuring the system's passivity and, consequently, stability, improving safety. Although these stabilizers can address the issues of stability, the natural cost would be the degraded fidelity of haptic/force field or degraded motion/energy tracking accuracy due to unavoidable energy dissipation. Thus, in the literature, several variations are proposed to reduce conservatism and optimize performance depending on the application. For example, assistive systems that render haptic/force fields are naturally nonpassive (needed to elevate the mechanical energy for delivery of assistance); thus, conventional passivity-imposing stabilizers can significantly diminish the delivery of needed assistive force fields.

As a result, there is a need for algorithmic stabilizers that can impose stability while guaranteeing high-fidelity of force interaction, specifically when the rendered force field has assistive components. In this regard, the authors have recently investigated the ability of human biomechanics to absorb interactional energy during pHRI when controlling for stiff and relaxed co-contraction of the muscles [18]–[20]. This knowledge is graphically visualized as an energetic passivity map and exploited in the design of biomechanically-aware passivity controllers that reduce the conservatism of the closed-loop passivity condition and enhance the fidelity of rendered haptic feedback [18]–[23]. However, current methods of measuring this passivity biomarker require an offline identification process before each operation, often conducted on different days. The identification process is time-consuming and can be challenging for subjects who are susceptible to fatigue. Therefore, it is imperative to reuse the prior knowledge regarding the energetic behavior of a user's biomechanics and avoid re-identification (recalibration), reducing the exhaustion,

X. Zhou, P. Paik, R. O'Keeffe, and S.F. Atashzar are with the Dept. of Electrical and Computer Engineering, New York University (NYU), New York, NY, 11201 USA. Atashzar is also with the Dept. of Mechanical and Aerospace Engineering, Biomedical Engineering, NYU WIRELESS Center, and NYU CUSP. This material is based upon work supported by the US National Science Foundation under grants no #2121391 and #2208189. The work is also supported in part by NYUAD CAIR Award #CG010.

* Zhou, Paik, and O'Keeffe contributed equally to this work and shared the first authorship.

† Corresponding author: Atashzar (f.atashzar@nyu.edu).

fatigue, and time of operation and enhancing the usability of biomechanically-aware controllers.

In order to investigate the aforementioned issue, in this paper, for the first time, we perform an interday test-retest statistical reliability study based on intraclass correlation coefficient analysis (ICC) [24], [25] on the passivity-based biomechanical energetic absorption capability of the human limb. The goal is to examine the reliability of the upper-limb passivity biomarker regarding the energetic characteristics to be extrapolated over various days of use. The study answers: (a) *whether the biomechanical energetic absorption capability of the human upper-limb is a consistent measurement and thus can be used reliably and repetitively* and (b) *how much variance exists in the identified passivity biomarker*. In this work, we also and specifically investigate *the dependency of reliability on the direction of pHRI and the level of muscle co-contraction*. During the identification process, subjects are asked to control the level of co-contraction through a biofeedback mechanism visualizing the muscle activities captured in real-time using a surface electromyography (sEMG) system from Delsys, Inc (MA, USA). The generated passivity biomarker in 8 different directions of interaction is named as MyoPassivity Map. Five healthy subjects were recruited for the study. The biomechanical absorption capabilities of the subjects are measured between two subsequent days and used for the reliability analysis. The statistical analysis indicates that the identified passivity map is highly reliable based on the intraclass correlation coefficient analysis within different days and various interactions. The results, for the first time, illustrate that a single session estimation of the energetic behavior (i.e., one-shot identification) is reliable to be used repeatedly for biomechanics-aware pHRI stabilization enhancing practicality in real-life scenarios.

II. Method

This section provides details regarding the method for estimating the proposed biomechanical absorption capability of interactional energy during physical human-robot interaction (for the human upper-limb), the corresponding ICC-based reliability assessment over two days of testing and retesting, and the experimental protocol.

A. Energetic Identification of Biomechanics during pHRI

In this work, we utilize the output strictly passive (OSP) definition rooted in the Strong Passivity formulation of nonlinear control theory [6] to characterize the energetic behavior of human upper-limb during physical human-robot interaction. The OSP definition allows us to calculate a lower bound on the amount of energy that can be absorbed by human biomechanics in different directions and muscle co-contraction levels. The OSP formulation in this context is given in (1).

$$\int_0^t F(t)^T V(t)dt + E(0) \geq \xi \int_0^t V(t)^T V(t)dt \qquad (1)$$

In (1), $F(t)$ is the force perturbation and the input into the human limb biomechanics. Also, $V(t)$ is the perturbation velocity response. Considering (1), ξ is the excess of passivity (EoP) of the human biomechanics, which will form a lower bound on the amount of energy that can be absorbed by human biomechanics during haptics-enabled pHRI. In this context, haptics-based pHRI relates to the kinesthetic interaction. Considering zero initial energy (i.e., $E(0) = 0$), the OSP formulation can be rearranged to calculate the EoP as:

$$\xi = \frac{\int_{T_s}^{T_e} F(t)^T V(t)dt}{\int_{T_s}^{T_e} V(t)^T V(t)dt}. \qquad (2)$$

The excess of passivity of human biomechanics, i.e., ξ, is recently considered as a potential energy reservoir [18]–[22] in our published stabilizers, such as [20], to increase the margin of stability and reduce the conservatism of the closed-loop pHRI system. We have studied the excess of passivity for the human ankle joint during human-exoskeleton interaction [18].

In this experiment, the participant's upper-limb was perturbed in eight directions of the X-Y plane, starting from 0 degrees and ending at 315 degrees in a counterclockwise order, as depicted in Fig. 1(IV). Before the experiment, each subject completed a familiarization phase which involved 2 minutes of practicing the perturbations. Each perturbation lasted for 10 s, during which the subject was provided with real-time feedback of their muscle co-contraction (biofeedback) and followed a guideline muscle co-contraction level while the robot perturbed the upper-limb and collected force and velocity information to estimate the corresponding energetic behavior.

During the experiment, the order of perturbation directions was the same for all participants to ensure similar experimental conditions. The maximum linear displacement of the perturbation was set to be 3 cm. Also, the maximum speed of the perturbation was 0.27 m/s. The perturbation position $P(t)$ is defined by a mixture of sinusoids, as follows:

$$P(t) = A(\frac{B + \Sigma_{i=1}^{5} a_i sin(\omega_i t + \phi_i)}{C})m \qquad (3)$$

where $\omega_1 = 2\pi, \omega_2 = 3\pi, \omega_3 = 4\pi, \omega_4 = 5\pi, \omega_5 = 6\pi$, $\phi_1 = \pi/2, \phi_2 = \pi/2, \phi_3 = 0, \phi_4 = \pi/2, \phi_5 = 0$ and $a_1 = 1, a_2 = 1, a_3 = 1, a_4 = 1, a_5 = 10$. A is the amplification factor which sets the amplitude scale of $P(t)$, B is an offset and C is a normalization factor. In this case, $A = 3cm$, $B = 11.44$ and $C = 24.18$. The corresponding velocity profile is:

$$V(t) = A(\frac{\Sigma_{i=1}^{5} a_i \omega_i cos(\omega_i t + \phi_i)}{C})m/s \qquad (4)$$

At the end of each perturbation, the robot returned to the zero/home position before proceeding to the next direction. For both co-contraction conditions, there was one trial of each perturbation direction during which several cyclic perturbations were provided. The last 5 seconds of the perturbation in each direction is used to calculate the EoP and avoid artifacts caused by transient directional changes. Therefore, in (2), T_s represents the beginning of the 5 s window, and T_e represents the end of the 5 s window during the identification phase.

B. Participants

Five healthy subjects (three males and two females, age: 28 ± 5 years) were recruited for this work. The study was approved by the New York University Institutional Review Board. Each subject signed a consent form prior to the

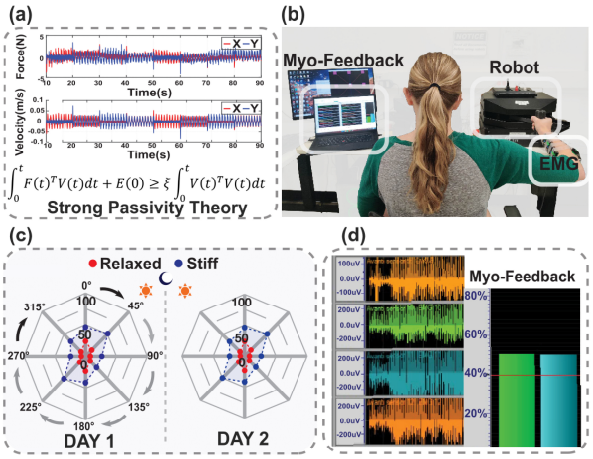

Fig. 1. (a) Example of reactive force and velocity profiles. (b) Identification process and set-up. (c) Resulting energetic passivity map in two sessions. (d) Real-time sEMG recording and visual myo-feedback.

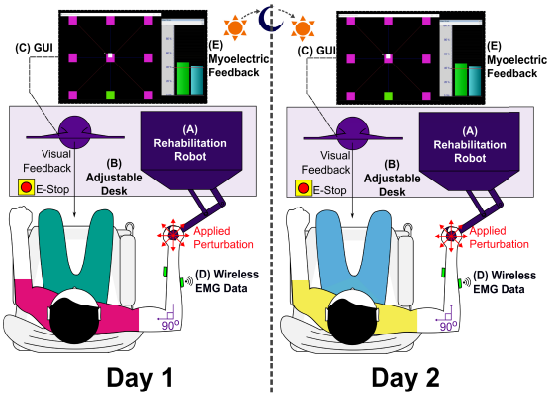

Fig. 2. Experimental set-up showing the: (A) Quanser rehabilitation robot, (B) height-adjustable table, (C) GUI, (D) Delsys wireless system, and (E) electromyographic biofeedback.

experiment and confirmed no history of any diagnosed/known neurological or motor damage or disorders. The demographic data is provided in Table I. The correlation between the demographic data and the proposed biomarker (i.e. EoP of biomechanics) is not investigated in this study but can be a topic of future work.

TABLE I
DEMOGRAPHIC DATA OF SUBJECTS

Subject	*Height (m)*	*Weight (kg)*	*Age*	*Sex*
1	1.77	64	24	M
2	1.62	58	24	M
3	1.70	57	24	F
4	1.87	77	32	M
5	1.73	62	33	F

C. Experimental Setup

In order to investigate the interday reliability of the upper-limb excess of passivity map under different interactional scenarios (two co-contraction levels and eight directions of interaction) over 2 days, a systematic identification protocol is designed (see the experiment flow in Fig. 1). The experimental set-up is shown in Fig. 2 and is composed of: (1) a 2-DOF Quanser upper-limb rehabilitation robot for biomechanical perturbation (from Quanser, Markham, ON, Canada), (2) a height-adjustable table to match the height of the user, (3) a visual graphical user interface (GUI) to provide visual information about the direction of the perturbation and visual biofeedback for the subject regarding the muscle co-contraction during perturbation, and (4) a 16-channel wireless Bipolar Delsys Trigno dry-electrode system (from Delsys, inc, MA, USA).

The needed information modalities for the identification of the energy absorption capacity of biomechanics, including input force and output velocity profiles besides muscle activities from 16 sEMG channels, are recorded in real-time and in-sync. The force and velocity are sampled at 500 Hz, and the sEMG signals are sampled at 2148 Hz. The experimental protocol is designed to assess the energetic characteristics of the user's upper-limb in eight geometric directions of interaction and two co-contraction conditions over two consecutive days (24 hours time gap). The subjects are requested to follow the prescribed co-contraction level while the robot perturbs their biomechanics. The collected data combined with the OSP math would allow us to investigate if the excess of passivity of the human upper-limb is a reliable measure of energetic behavior and can be used to estimate the energy absorption capacity with one day of observation.

Before the experiment, the table height is adjusted to allow for implementing the same prescribed posture for all users while estimating the EoP. The angle between the arm and torso is set to be about 45 degrees when the user is holding the robot handle. The chair is located so that the upper and lower parts of the arm make a 90-degree angle when the end-effector is at the center of the workspace, as provided by the GUI. During the identifcation period, the maximum voluntary contraction (MVC) is measured at the extensor digitorum and palmaris longus muscles. It should be noted that these two muscles are selected based on their sensitivity to the co-contraction in the forearm, especially during physical human-robot interaction.

The subjects maintained the required co-contraction levels with the assistance of visual myofeedback from their sEMG signals at a desired level of 5%MVC for relaxed and 40%MVC for stiff co-contraction condition. At the beginning of the experiment, first, the subject is instructed to grasp the handle with maximum effort and the MVC is recorded as the maximum root mean square (RMS) value of the sEMG signal at each muscle. During the experiment, the %MVC at each muscle is measured by normalizing the current RMS of the sEMG to the recorded MVC. The %MVC indicates the percentage of the participant's maximum co-contraction level and is used as a visual bio-feedback for the participant during the experiment. It should be noted that the provided bio-feedback is subject-specific (considering the MVC normalization) and immune to variation in the sEMG magnitude across participants. More muscle co-contraction (caused by a tighter grasping of the robot handle) will result in a higher %MVC. Two co-contraction conditions were defined based on the desired %MVC: (a) relaxed holding of the robot handle with 5%MVC and (b) stiff co-contraction maintaining approximately 40%MVC. The order of the conditions is randomized.

As mentioned, during the experiment, the user is asked to hold the robot's handle and let the robot perturb the limb while maintaining the prescribed contractions. At the start of the experiment, the robot moves the user's hand to the center

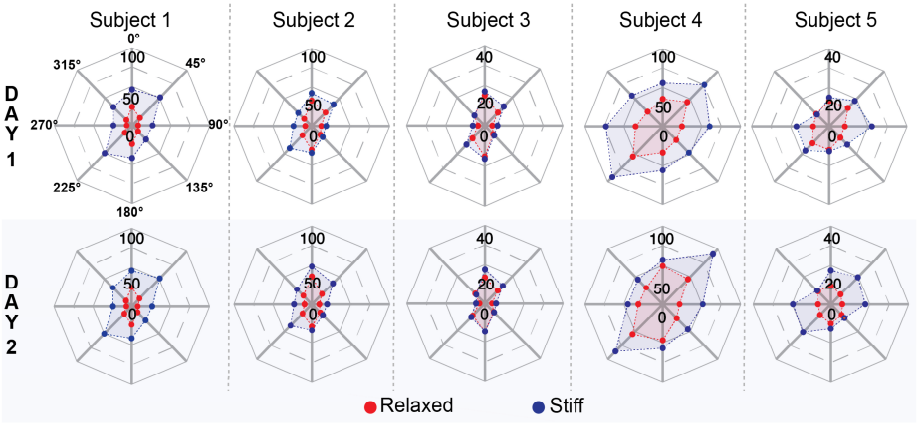

Fig. 3. Resulting Geometric MyoPassivity Maps for all subjects during Day 1 (top) and Day 2 (bottom). The red dots represent the EoP of the relaxed condition, and the blue dots represent the stiff conditions. The EoP values in eight geometric directions (0°, 45°, 90°, 135°, 180°, 225°, 270°, 315°) is shown.

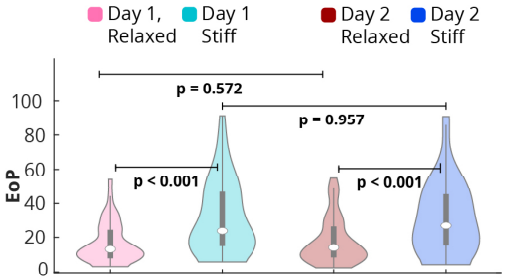

Fig. 4. Violin plots comparing the EoP between days and grasp conditions. For a given day and grasp condition, the EoP of all five subjects in all eight directions was combined together into a single distribution ($n = 8 \times 5 = 40$). For both days, the EoP was significantly higher for the stiff than relaxed condition (*Wilcoxon signed-rank:* $p - value < 0.001$). For both the relaxed and stiff conditions, no significant difference between Day 1 and Day 2 was observed (*Wilcoxon signed-rank:* $p - value > 0.571$).

location shown on the GUI. The robot begins to perturb the limb in eight directions separately, where the biomechanical energetic absorption capability is calculated in real-time using the force and velocity information and the OSP formulation. This procedure is repeated for the second co-contraction condition. Before the second co-contraction condition, there was a five-minute break for the subject to rest. The experiment is then conducted 24 hours later using the same protocol.

D. Test-retest Reliability

In this work, in order to assess the reliability of the proposed energetic measure of the upper-limb, the intraclass correlation coefficients were evaluated, analyzing the between-session test-retest reliability [24], [25]. The reliability of the EoP measurements in this paper was interpreted from the ICC values with Fleiss' scale [26]. Fleiss' scale for interpreting reliability from the ICC values is a standard commonly used in the literature [27]–[30], and is explained as follows: poor reliability ($ICC < 0.4$), fair reliability ($0.4 < ICC < 0.75$), or excellent reliability ($ICC > 0.75$). Fleiss' scale has been applied in previous studies to convert raw ICC values into meaningful interpretations of reliability, notably in the context of biometrics [27]–[30]. In this work, the ICC values were calculated using the SPSS software (version 28, IBM Corp., Armonk, NY). The ICC was calculated with the fixed column and random row effects model, single score ($ICC(C,1)$) [25], [31]. $ICC(C,1)$ indicates the level of consistency between the two sessions and can be interpreted here as the reliability of the measurement obtained from a single session [24], [25]. $ICC(C,1)$ was calculated from a data matrix in the standard format presented by McGraw and colleagues with the subjects on the rows and the sessions on the columns [25], as illustrated in Table II. Each element of the data matrix X represents the energetic biomechanical capacity for the i^{th} subject in a given session. The $ICC(C,1)$ was computed for each co-contraction condition and direction.

TABLE II
DATA MATRIX FORMAT FOR THE CALCULATION OF BETWEEN-SESSION RELIABILITY WITH $ICC(C,1)$.

Subject	*Session 1*	*Session 2*
1	X_{11}	X_{12}
...	...	...
i	X_{i1}	X_{i2}
5	X_{51}	X_{52}

III. Results

The Geometric MyoPassivity maps of each subject for both co-contraction conditions on Day 1 and Day 2 of the experiment are shown in Fig. 3. The blue dots represent the identified EoP values for stiff conditions, whereas the red dots represent the identified EoP values for relaxed conditions. Following the same identification protocol, the first row displays the MyoPassivity map of five subjects collected on Day 1, and the second row displays the MyoPassivity map of five subjects acquired on Day 2. Detailed objective statistical evaluation using ICC is provided later in this section. However, as the first step, through visual inspection and as can be seen in Fig. 3, on both days, the EoP values of the stiff condition appear to be higher than the EoP values of the relaxed condition in each direction for almost all subjects (4 out of 5). This phenomenon is expected since higher muscle co-contractions have been linked to increases in the limb's intrinsic mechanical impedance. Fig. 3 shows that this phenomenon has enhanced the energy absorption capability of the biomechanics during the interaction with the robot, identified by the EoP in this paper over two days. Interestingly, differences were observed in the shape and magnitude of the MyoPassivity maps amongst subjects, for example Subject 3 has a maximum EoP of <20 Ns/m while Subject 4 has a maximum EoP of >125 Ns/m (Fig.

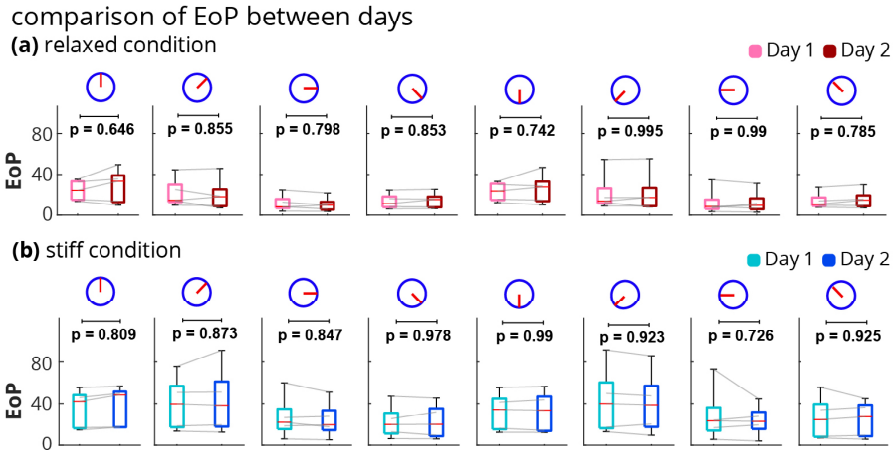

Fig. 5. **(a)** No significant difference was observed between the EoP distributions of day 1 and day 2 for any direction within the relaxed condition ($p > 0.645$). **(b)** No significant difference between Day 1 and Day 2 was uncovered for the directions within the stiff condition ($p > 0.724$).

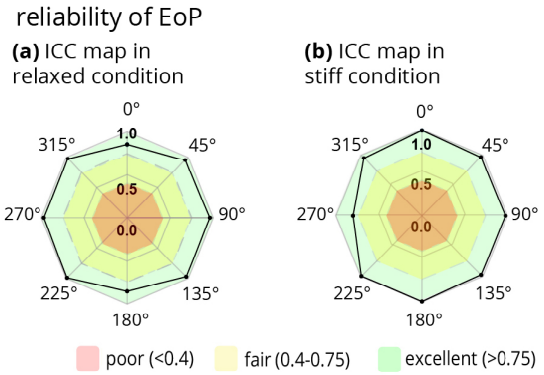

Fig. 6. ICC maps indicate excellent reliability in all directions for either grasp condition. The $ICC(C,1)$ value is shown as a black dot in the map for each direction. The shaded regions indicate poor, fair, and excellent reliability, depending on the $ICC(C,1)$ value, according to Fleiss' scale [26]. **(a)** $ICC(C,1) \geq 0.85$ in all directions for the relaxed condition. **(b)** $ICC(C,1) \geq 0.8$ in all directions for the stiff condition.

TABLE III
$ICC(C,1)$ VALUES FOR EACH CONDITION AND DIRECTION

	Grasp Condition	
Direction	*Relaxed*	*Stiff*
0°	0.85	0.99
45°	0.95	0.97
90°	0.96	0.97
135°	0.97	0.97
180°	0.86	1.00
225°	0.99	0.99
270°	0.97	0.80
315°	0.97	0.95

3). However, the shape is well-maintained between Day 1 and Day 2 for each subject regarding the muscle co-contraction levels resulting in high reliability of this measure. This means that in each geometric direction of the passivity map, the estimated EoP value indicates a level of reproducibility and therefore shows potential promise that the user-specific MyoPassivity maps can be used reliably between days, and this is statistically evaluated in more detail below.

In Fig. 4, changes of EoP with respect to alternation of muscle co-contraction and interday variability are investigated. For this, the EoP values of all subjects are combined and then separated into four groups: Day 1 Relaxed, Day 1 Stiff, Day 2 Relaxed, and Day 2 Stiff. The resulting violin plot distributions of the four groups are presented in Fig. 4. It should be noted that each distribution in Fig. 4 consists of the EoP values for each of the five subjects in all eight directions ($n = 5 \times 8 = 40$ for each violin plot). Statistical analysis was conducted with respect to the relaxed-stiff, relaxed-relaxed, and stiff-stiff groups across the two days. Through the Kolmogorov-Smirnov normality tests [32], the distributions were found to be non-normal. Therefore, the Wilcoxon signed-rank test [33] was used to evaluate the null hypothesis (significance threshold: $p - value = 0.05$). The results show that the stiff co-contraction condition leads to a higher EoP on both Day 1 and Day 2 (*Wilcoxon signed-rank:* $p - value < 0.001$). Additionally, no statistically significant difference was observed between the relaxed distributions of Day 1 when compared with Day 2 (*Wilcoxon signed-rank:* $p - value = 0.572$). Also, no significant difference was observed between the stiff distributions of Day 1 when compared with Day 2 (*Wilcoxon signed-rank:* $p - value = 0.957$). The results validate the observed behavior of the MyoPassivity maps showing that the stiff EoP values are significantly higher than the relaxed EoP values, as was also observed in Fig. 3.

The change of the EoP values between days was also investigated in each geometric direction for a given co-contraction condition. The EoP values of the five subjects are compared between Day 1 and Day 2 in Fig. 5 ($n = 5$). Gray lines connect EoP values of the same subject from Day 1 to Day 2. No statistically significant difference was observed between Day 1 and Day 2 in any direction, and this observation was the same for both co-contraction conditions ($p - value > 0.645$).

After observing no significant difference between EoP values across days, a formal reliability analysis was conducted. This is the most important result of the paper. The intraclass correlation coefficient in each direction for relaxed and stiff conditions are calculated and visualized in Fig. 6 and provided in Table III. The analysis showed $ICC(C,1) \geq 0.8$ in all directions for both co-contraction conditions. This result, for the first time, reveals that the EoP measurement has statistically excellent reliability ($ICC > 0.75$) for the tested direction of pHRI and for both conditions of muscle co-contraction. The results suggest that the biomechanical absorption capability, assessed by the calculated EoP in this paper, is a consistent

measure in the tested geometric directions and can be used reliably and repeatedly with minimal need for recalibration based on a one-shot observation for each subject. In other words, this work, for the first time, suggests that the MyoPassivity map acts as an energetic "signature" of the user's biomechanics. The exploitation of this in the design of biomechanics-aware control algorithms can significantly reduce the time needed for data collection and recalibration, reducing fatigue and exhaustion. This can be directly applied to biomechanics-aware pHRI systems, such as telerobotic rehabilitation, upper-limb robotic exoskeletons, robotic ankle orthoses, and haptics-enabled telerobotic surgery.

IV. Conclusion

In this paper, an interday test-retest statistical reliability study of the upper-limb MyoPassivity map is performed for the first time during physical human-robot interaction. The proposed map represents the biomechanical energetic absorption capability and can be used in pHRI stabilization schemes enhancing performance and haptics/force transparency while imposing stability. However, without ensuring reliability, there would be a need for data collection and (re)calibration prior to each time of pHRI operation. This would be exhaustive, time-consuming, and could challenge subjects susceptible to fatigue. It is beneficial to remove the identification process for consecutive uses and reuse the unique MyoPassivity "signature", reducing the time, exhaustion, and fatigue. The results of the reliability study conducted by ICC analysis, investigated for the first time in this paper, indicate that the identified MyoPassivity maps have statistically excellent interday reliability ($ICC > 0.75$) in different geometric directions and co-contraction levels.In addition, no statistically significant difference was observed between the identified MyoPassivity maps on different days in all eight geometric directions and grasp conditions ($p > 0.645$). The robustness of the MyoPassivity map as a measurement is demonstrated by the excellent ICC-based reliability across all task conditions despite differences in the shape and magnitude of the maps amongst subjects. Thus, it can be concluded that the energetic passivity map created in a one-shot observation represents the unique user-specific biomechanic signature, which is reliable and can be used repeatedly, especially for biomechanics-aware pHRI to enhance the haptics rendering experience while regarding the safety of the human user. The future line of work includes: (a) enhancing and generalizing the study across more participants and days to further investigate the reliability and (b) determining the reliability of the MyoPassivity map under other conditions beyond geometric directions and co-contraction levels.

References

[1] H. S. Lo and S. Q. Xie, "Exoskeleton robots for upper-limb rehabilitation: State of the art and future prospects," *Medical engineering & physics*, vol. 34, no. 3, pp. 261–268, 2012.

[2] S. Avgousti *et al.*, "Medical telerobotic systems: current status and future trends," *Biomedical engineering online*, vol. 15, no. 1, pp. 1–44, 2016.

[3] M. Shahbazi *et al.*, "Robotics assisted mirror rehabilitation therapy: A therapist-in-the-loop assist-as-needed architecture," *IEEE/ASME Transactions on Mechatronics*, vol. 21, no. 4, pp. 1954–1965, 2016.

[4] D. Shi *et al.*, "A review on lower limb rehabilitation exoskeleton robots," *Chinese Journal of Mechanical Engineering*, vol. 32, pp. 1–11, 2019.

[5] M. Vidyasagar, *Nonlinear Systems Analysis*. SIAM, 2002.

[6] A. Jazayeri *et al.*, "Stability analysis of teleoperation systems under strictly passive and non-passive operator," in *2013 World Haptics Conference (WHC)*, 2013, pp. 695–700.

[7] D. Hill and P. Moylan, "Stability results for nonlinear feedback systems," *Automatica*, vol. 13, no. 4, pp. 377–382, 1977.

[8] S. Haddadin and E. Croft, "Physical human–robot interaction," in *Springer handbook of robotics*. Springer, 2016, pp. 1835–1874.

[9] V. der Loos *et al.*, "Rehabilitation and health care robotics," in *Springer handbook of robotics*. Springer, 2016, pp. 1685–1728.

[10] M. Shahbazi *et al.*, "A systematic review of multilateral teleoperation systems," *IEEE transactions on haptics*, vol. 11, pp. 338–356, 2018.

[11] M. Laghi *et al.*, "Unifying bilateral teleoperation and tele-impedance for enhanced user experience," *The International Journal of Robotics Research*, vol. 39, no. 4, pp. 514–539, 2020.

[12] H. Choi *et al.*, "Chattering-free time domain passivity approach," *IEEE Transactions on Haptics*, vol. 15, no. 3, pp. 572–581, 2022.

[13] J.-H. Ryu *et al.*, "A passive bilateral control scheme for a teleoperator with time-varying communication delay," *Mechatronics*, vol. 20, no. 7, pp. 812–823, 2010.

[14] V. Chawda and M. K. O'Malley, "Position synchronization in bilateral teleoperation under time-varying communication delays," *IEEE/ASME Transactions on Mechatronics*, vol. 20, no. 1, pp. 245–253, 2015.

[15] S. F. Atashzar *et al.*, "A small-gain approach for nonpassive bilateral telerobotic rehabilitation: Stability analysis and controller synthesis," *IEEE Transactions on Robotics*, vol. 33, no. 1, pp. 49–66, 2017.

[16] J.-H. Ryu *et al.*, "Time domain passivity control with reference energy following," *IEEE Transactions on Control Systems Technology*, vol. 13, no. 5, pp. 737–742, 2005.

[17] B. Hannaford and J.-H. Ryu, "Time-domain passivity control of haptic interfaces," *IEEE Transactions on Robotics and Automation*, vol. 18, no. 1, pp. 1–10, 2002.

[18] S. F. Atashzar *et al.*, "Energetic passivity decoding of human hip joint for physical human-robot interaction," *IEEE Robotics and Automation Letters*, vol. 5, no. 4, pp. 5953–5960, 2020.

[19] S. F. Atashzar *et al.*, "A grasp-based passivity signature for haptics-enabled human-robot interaction: Application to design of a new safety mechanism for robotic rehabilitation," *The International Journal of Robotics Research*, vol. 36, no. 5-7, pp. 778–799, 2017.

[20] P. Paik *et al.*, "Power-based velocity-domain variable structure passivity signature control for physical human-(tele)robot interaction," *IEEE Transactions on Robotics*, pp. 1–13, 2022.

[21] S. F. Atashzar *et al.*, "A passivity-based approach for stable patient–robot interaction in haptics-enabled rehabilitation systems: modulated time-domain passivity control," *IEEE Transactions on Control Systems Technology*, vol. 25, no. 3, pp. 991–1006, 2016.

[22] S. Thudi and S. F. Atashzar, "Discrete windowed-energy variable structure passivity signature control for physical human-(tele)robot interaction," *IEEE Robotics and Automation Letters*, vol. 6, no. 2, pp. 3647–3654, 2021.

[23] X. Zhou *et al.*, "Upper-limb geometric myopassivity map for physical human-robot interaction," *arXiv preprint arXiv:2302.00495*, 2023.

[24] P. E. Shrout and J. L. Fleiss, "Intraclass correlations: Uses in assessing rater reliability," *Psychol. Bull.*, vol. 86, no. 2, pp. 420–428, Mar. 1979.

[25] K. O. McGraw and S. P. Wong, "Forming inferences about some intraclass correlation coefficients," *Psychol. Methods*, vol. 1, no. 1, pp. 30–46, Mar. 1996.

[26] J. L. Fleiss, *Design and Analysis of Clinical Experiments*. John Wiley & Sons, Jan. 2011.

[27] S. M. Khoddami *et al.*, "Validity and reliability of surface electromyography in the assessment of primary muscle tension dysphonia," *J. Voice*, vol. 31, no. 3, pp. 386.e9–386.e17, May 2017.

[28] N. J. Erickson *et al.*, "Koos classification of vestibular schwannomas: A reliability study," *Neurosurgery*, vol. 85, no. 3, pp. 409–414, Sep. 2019.

[29] L. M. Volland *et al.*, "Development and reliability of the joint tissue activity and damage examination for quantitation of structural abnormalities by musculoskeletal ultrasound in hemophilic joints," *J. Ultrasound Med.*, vol. 38, no. 6, pp. 1569–1581, Jun. 2019.

[30] M. D. Fabio Antonaci, "Pressure algometry in healthy subjects: inter-examiner variability," *Scand. J. Rehabil. Med.*, vol. 30, no. 3, p. 8, 1998.

[31] J. J. Bartko, "On various intraclass correlation reliability coefficients," *Psychol. Bull.*, vol. 83, no. 5, pp. 762–765, Sep. 1976.

[32] H. W. Lilliefors, "On the Kolmogorov-Smirnov test for normality with mean and variance unknown," *Journal of the American statistical Association*, vol. 62, no. 318, pp. 399–402, 1967.

[33] R. F. Woolson, "Wilcoxon signed-rank test," *Wiley encyclopedia of clinical trials*, pp. 1–3, 2007.